

Anderson localization of electromagnetic waves in three dimensions

Alexey Yamilov^{1*}, Sergey E. Skipetrov², Tyler W. Hughes³, Momchil Minkov³,
Zongfu Yu^{3,4,†}, Hui Cao^{5*}

¹Physics Department, Missouri University of Science & Technology, Rolla, Missouri 65409

²Univ. Grenoble Alpes, CNRS, LPMCM, 38000 Grenoble, France

³Flexcompute Inc, 130 Trapelo Road, Belmont, MA, 02478

⁴Department of Electrical & Computer Engineering, University of Wisconsin, Madison, WI, 53705

⁵Department of Applied Physics, Yale University, New Haven, Connecticut 06520

* yamilov@mst.edu

† zongfu@flexcompute.com

* hui.cao@yale.edu

March 8, 2022

Anderson localization marks a halt of diffusive wave propagation in disordered systems. Despite extensive studies over the past 40 years, Anderson localization of light in three dimensions has remained elusive, leading to the questions about its very existence. Recent orders-of-magnitude speed-up of finite-difference time-domain calculations allows us to conduct brute-force numerical simulations of light transport in fully disordered 3D systems with unprecedented size and refractive index contrast. We demonstrate three-dimensional localization of vector electromagnetic waves in random packings of perfect electric conductor spheres, in sharp contrast to the absence of localization for dielectric spheres with a refractive index contrast up to 10. Our work opens

a wide range of avenues in both fundamental research related to Anderson localization and potential applications using 3D localized states.

Anderson localization (AL) (1) is an emergent phenomenon for both quantum and classical waves including electron (2–4), cold-atom (5, 6), electromagnetic (EM) (7–11), acoustic (12, 13), water (14), seismic (15), and gravity (16) waves. Unlike in one or two dimensions, AL in three dimensions (3D) requires strong disorder (1, 17, 18). A mobility edge separating the diffuse transport regime from AL can be estimated from the Ioffe-Regel criterion $k_{\text{eff}} \ell_s \sim 1$, where k_{eff} is the effective wavenumber in the medium and ℓ_s is the scattering mean free path (19). This criterion suggests two avenues to achieving localization: reduction of k_{eff} or ℓ_s . For EM waves, the former is realized by introducing partial order or spatial correlation in scatterer positions (7, 20). In comparison, reaching localization of light in fully random photonic media by increasing scattering strength (decreasing ℓ_s) turns out to be much more challenging (21, 22). Despite successful experiments in low-dimensional systems (9, 10, 23), 3D localization remained stubbornly elusive (24), which triggered theoretical (25, 26) and experimental (27) studies of the reasons that impede it.

Anderson himself originally proposed “*a system composed essentially of random waveguides near cut-off and random resonators, such as might be realized by a random packing of metallic balls of the right size*” as “*the ideal system*” for localization of EM radiation (8). In practice, the absorption of metals obscures localization (9, 28), and the experimental focus shifted to dielectric materials with low loss and high refractive index (28–32). However, even for dielectric systems, experimental artifacts due to residual absorption and inelastic scattering mar the data (21, 22). Numerically these artifacts can be excluded, but 3D random systems of sufficiently large size and high refractive index contrast could not be simulated due to an extraordinarily long computational time required (33, 34).

Recent implementation of the finite-difference time-domain (FDTD) algorithm on emerging

computing hardware has speed-up calculations by a factor of 100 (35, 36). Using this highly-efficient hardware-optimized method, we solve the Maxwell equations by brute force in 3D. It enables us to simulate sufficiently large systems and high refractive index contrast to address the following questions: can 3D AL of EM waves be achieved in fully random systems of dielectric scatterers? If not, can it occur in any other systems without aid of spatial correlations?

Answering these long-standing questions would not only address the fundamental aspects of wave transport and localization across multiple disciplines, but also open new research avenues. For example, in topological photonics (37), the interplay between disorder and topological phenomena may be explored beyond the limit of weak disorder in low-dimensional systems (38). Also in cavity quantum electrodynamics with Anderson-localized modes (39), going 3D would avoid the out-of-plane losses inherent for 2D systems and cover the full angular range of propagation directions (40). In addition to fundamental studies, disorder and scattering has been harnessed for various photonic device applications, but mostly with diffuse waves (41). Anderson-localized modes can be used for 3D energy confinement to enhance optical nonlinearities, light-matter interactions, and control random lasing as well as targeted energy deposition.

We first consider EM wave propagation through a 3D slab of randomly packed lossless dielectric spheres of radius $r = 100$ nm and refractive index $n = 3.5$. This corresponds to the highest index contrast achieved experimentally in optical range with porous GaP around the wavelength $\lambda_0 = 650$ nm in the vicinity of the first Mie resonance of an isolated sphere, see Methods. To avoid spatial correlations, the sphere positions are chosen completely randomly, leading to spatial overlap where index is capped at the same value of n . To avoid reflection at the interfaces of the slab, we surround it by a uniform medium with the refractive index equal to the effective index of the slab, $n_{\text{eff}} = [(1 - f) + fn^2]^{1/2}$, for a given sphere volume fraction f , c.f. Fig.1a. As described in Methods, for each wavelength, we compute the scattering mean

free path ℓ_s directly from the rate of attenuation of co-polarized field with depth. This, together with the effective wavenumber $k_{\text{eff}} = n_{\text{eff}}(2\pi/\lambda)$, gives the Ioffe-Regel parameter shown in Fig. 1c. It features a minimum around $\lambda = 650$ nm, and the smallest value of $k_{\text{eff}}\ell_s \simeq 0.9$ is reached at $f = 38\%$. We also compute the transport mean free path ℓ_t from continuous wave (CW) transmittance of an optically thick slab with thickness $L > 20\ell_t$, see Methods. In Fig. 1d, $k_{\text{eff}}\ell_t$ also exhibits a dip in the same wavelength range as $k_{\text{eff}}\ell_s$, however, the smallest $k_{\text{eff}}\ell_t$ is found at lower f of 18–29%, as the dependent scattering sets in at higher f . In search for AL in this wavelength range, we numerically simulate propagation of a narrow-band Gaussian pulse centered at $\lambda = 650$ nm with plane wavefront, and compute the transmittance through the slab $T(t)$ as a function of arrival time t . The diffusive propagation time t_D approximately corresponds to the arrival time of the peak in Fig. 1e. At $t \gg t_D$, the decay of the transmitted flux is exponential over 12 orders of magnitude, as expected for purely diffusive systems (42). Rate of this exponential decay is equal to $1/t_D$, which is directly related (42) to the smallest diffusion coefficient within the spectral range of the excitation pulse, see Methods. In Fig. 1f, the dependence of this diffusion coefficient D on the dielectric filling fraction f exhibits a minimum at $f \sim 30\%$. Inset in Fig. 1e shows that the further increase of the sample thickness does not lead to any deviation from diffusive transport. At $t \gg t_D$, the spatial intensity distribution inside the sample features a depth profile (averaged over cross-section) equal to that of the first eigenmode of the diffusion equation in Fig. 1b. We therefore rule out a possibility of AL in uncorrelated ensembles of dielectric spheres with $n = 3.5$.

At microwave frequencies, the refractive index may be even higher than $n = 3.5$. We therefore, perform numerical simulation for a similar 3D slab of dielectric spheres with $n = 10$. The main results are summarized here, and details are presented in Supplementary Information (SI). A large scattering cross section $\sigma_s(\lambda)$ of a single sphere near the first Mie resonance leads to strong dependent scattering already at small filling fractions. We find the Ioffe-Regel parameter

$k_{\text{eff}} \ell_s \gtrsim 1$ despite the very high refractive index contrast. This is attributed to dependent scattering that becomes significant even at relatively low dielectric filling fraction. Furthermore, the numerically calculated $T(t)$ for $L/\ell_t \gg 1$ does not exhibit any deviation from diffusive transport: at $t \gg t_D$, the decay of transmittance is still exponential over ~ 10 orders of magnitude. In addition, scaling of CW transmittance with the inverse slab thickness $1/L$ remains linear for all f , as expected for diffusion, see SI. We therefore conclude that AL does not occur in random ensembles of dielectric spheres, thus closing the debate about the possibility of light localization in a white paint (8, 22).

Previous studies (25, 26) suggest that absence of AL for EM waves may be due to longitudinal waves that exist in a heterogeneous dielectric medium, where the transversality condition $\nabla \cdot \mathbf{E}(\mathbf{r}) = 0$ does not follow from the Gauss's law $\nabla \cdot [\epsilon(\mathbf{r})\mathbf{E}(\mathbf{r})] = 0$, because of the position dependence of $\epsilon(\mathbf{r})$. Here, we propose to eliminate longitudinal waves and realize AL of EM waves by using perfectly conducting spheres as scatterers. No electric field penetrates inside a perfect electric conductor (PEC) and EM waves are purely transversal wherever their amplitude is non-zero. The volume of PEC spheres is simply excluded from the free space and becomes unavailable for light. Thus, at high PEC volume fraction, light propagates in a random network of irregular air cavities and waveguides formed by the overlapping PEC spheres, akin to the original proposal of Anderson (8).

Similarly to the dielectric systems above, we simulate a 3D slab composed of randomly packed, overlapping PEC spheres of radius $r = 50$ nm in air. Figure 2 shows the results of simulating an optical pulse propagating through $10\mu\text{m} \times 10\mu\text{m} \times 3.3\mu\text{m}$ slabs of various PEC fractions. $T(t)$ displays non-exponential tails at high fractions $f = 41\%$, 48% in Fig. 2a. From the decay rate obtained via a sliding-window fit, we extract a time-dependent diffusion coefficient $D(t)$, c.f. Fig. 2b, which shows a power-law decay with time, as predicted by the self-consistent theory of localization (43). The non-exponential decay of $T(t)$ and the time-dependence of D

are the signatures of AL (13, 43). In contrast, at lower PEC fractions $f = 8\%$, 15% , D is independent of time. Figure 2c reveals a transition from time-invariant D to time-dependent $D(t)$ around $f = 33\%$ when $D(t)$ starts deviating from a constant. Using Fourier transform, we compute the spectrally resolved transmittance $T(\lambda)$. Figures 2d,e contrast the transmission spectra $T(\lambda)$ of diffusive and localized samples. The former features smooth, gradual variations with λ due to broad overlapping resonances, whereas the latter exhibits strong resonant structures consistent with the average mode spacing exceeding the linewidth of individual modes, in accordance with Thouless criterion of localization: the spectral narrowing of modes is intimately related to their spatial confinement (3, 9, 44). Color maps in Figs. 2d,e show spatial intensity distributions inside the sample, $\langle I(x, y_0, z; \lambda) \rangle_x$, averaged over x for a cross-section $y = y_0$. These two-dimensional maps contrast slow variation with z and λ in the diffusive system (panel d) to the sharp features due to spatially-confined modes in the localized system (panel e). Furthermore, there exist ‘necklace’ states with multiple spatially separated intensity maxima, originally predicted for electrons in metals (45).

Insight into the mechanism behind AL in the random ensemble of PEC spheres can be obtained from the wavelength dependence of the Ioffe-Regel parameter $k\ell_s$. We compute it using a procedure similar to that in dielectrics, see Methods. At sufficiently large PEC volume fraction, ℓ_s becomes essentially independent of wavelength in the range of size parameter kr of PEC spheres in Fig. 3a. Consequently, the Ioffe-Regel parameter acquires $1/\lambda$ dependence as seen in Fig. 3b. It drops below the value of unity within the excitation pulse bandwidth $\lambda \simeq 650 \text{ nm} \pm 45 \text{ nm}$ for f between 25% and 33% , in agreement with Fig. 2. To further verify the consistency of our results with the Ioffe-Regel criterion, we conduct a finite-size scaling study. We compute the dependence of CW transmission T on the slab thickness L , see Methods. Figure 3c shows the logarithmic derivative $d \log(T)/d \log(L)$ as a function of $k\ell_s$. In the diffusive regime, Ohm’s law $T \propto 1/L$ is expected, leading to a scaling power of -1 , as

indeed observed for $k\ell_s > 1$. Around $k\ell_s \sim 1$ we see a departure from $1/L$ scaling of transmittance. Note that the scaling theory of localization (46) predicts a single-parameter scaling with the dimensionless conductance g but not with $k\ell_s$. Estimating the number of transverse modes as $N = 2\pi(L/\lambda)^2(1-f)^{2/3}$ for $L \times L$ area of the slab, we compute $g = TN$ (47) and $\beta(g) \equiv d\log(g)/d\log(L)$. Figure 3d shows a good agreement between the numerical data and the model function $\beta(g) = 2 - (1+g)\log(1+g^{-1})$ (47). In diffusive regime $g > 1$, $\beta(g) \rightarrow 1$; whereas in the localized regime $g < 1$, $\beta(g) \propto \log(g)$. The latter is a manifestation of the exponential scaling of g with L in the regime of Anderson localization.

To obtain the ultimate confirmation of AL of light in PEC composites, we simulate dynamics of the transverse spreading of a tightly focused pulse—a measurement that has been widely adopted in localization experiments (13, 32, 48). A pulse centered at $\lambda = 650$ nm with a bandwidth of 90 nm is focused to a small spot of area $\simeq 0.5 \mu\text{m}^2$ at the front surface of a wide 3D slab of dimensions $33\mu\text{m} \times 33\mu\text{m} \times 3.3\mu\text{m}$, c.f. Fig. 4a. We compute the transverse extent of intensity profile at the back surface of the slab. For a diffusive PEC slab with $f = 15\%$, we observe a rapid transverse spreading of light with time in Fig. 4b, which approaches the lateral boundary of the slab within ~ 2 ps. In sharp contrast, in the localized regime in Fig. 4c ($f = 48\%$), the transmitted intensity profile remains transversely confined even after 20 ps. This time corresponds to a free space propagation of 6 mm, which is ~ 2000 times longer than the actual thickness of the slab. Figure 4d quantifies this time evolution with the output beam diameter $d(t) = 2[\text{PR}(t)/\pi]^{1/2}$, where $\text{PR}(t) = [\int \int I(x, y, L; t) dx dy]^2 / \int \int I(x, y, L; t)^2 dx dy$ is the intensity participation ratio. For a diffusive slab, $d(t) \propto t^{1/2}$, while in the localized regime, $d(t)$ saturates at a value of the order of slab thickness L . Further evidence of AL include non-linear depth profile and strong non-Gaussian fluctuations of intensity inside the sample, see SI. We also confirm our results by repeating calculations for a 3D slabs of PEC spheres with larger radius $r = 100$ nm, and obtaining similar scaling behavior, c.f. SI, as in Figs. 3cd.

The striking difference between light propagation in dense random ensembles of dielectric and PEC spheres cannot be accounted for by the Ioffe-Regel parameter, as both reach $k_{\text{eff}}\ell_s \sim 1$ for similar values of the size parameter kr (Figs. 1c, 3b). Besides the absence of longitudinal fields in PEC composites, additional differences with respect to dielectric media facilitate Anderson localization in PEC. Starting from low scatterer number densities ρ , strong backscattering from isolated PEC spheres (49) results in a strongly anisotropic angular scattering diagram and $\ell_t < \ell_s$, which is very different from the situation for dielectric spheres. At higher ρ , groups of closely-spaced PEC particles create strong red-shifted resonances, see SI, leading to ℓ_s well below the independent scattering approximation (ISA) $\ell_s(\lambda) = 1/\rho\sigma_s(\lambda)$ for long wavelengths λ , see Fig. 3a for $f = 8\%$. Even when the gap in-between two PEC spheres is much narrower than λ , light scattering is resonantly enhanced for $kr < 1$, see SI. Additional voids formed by three or more PEC spheres create scattering resonances with similar properties that strengthen the effect, see internal field distributions in SI. The nearly dispersionless scattering mean free path ℓ_s below the ISA prediction is in stark contrast to the case of dielectric spheres for which scattering strongly decreases for $kr < 1$ (Rayleigh limit) and saturates with an increase of ρ due to dependent scattering. Eventually as the PEC filling fraction approaches 1, air voids no longer percolate through the system anymore, and a PEC composite becomes a perfect mirror. In our simulations, Anderson localization is observed at PEC fractions well below the air percolation threshold. Therefore, air voids are still connected by narrow propagation channels in which interference effects are enhanced due to the spatial confinement. Obviously, this regime is not accessible in a dielectric composite that becomes transparent in the limit of filling fraction approaching unity.

In summary, we report a large-scale microscopic simulation of EM wave propagation in 3D uncorrelated random ensembles of spheres, enabled by a vastly improved implementation of FDTD algorithm. Our results show no sign of Anderson localization for dielectric spheres with

refractive indices $n = 3.5$ and 10 . This may explain multiple failed attempts of experimental observation of AL of light in 3D dielectric systems over the last three decades (21, 22, 30–32). At the same time, we report the first numerical evidence of the possibility of AL of EM waves in random ensembles of PEC spheres over a broad spectral range. Localization is confirmed by eight criteria: the Ioffe-Regel criterion, the Thouless criterion, non-exponential decay of transmittance under pulsed excitation, vanishing of the diffusion coefficient, existence of spatially localized states, scaling of conductance, arrest of the transverse expansion of a narrow beam, and enhanced non-Gaussian fluctuations of intensity. Our study calls for renewed experimental efforts to be directed at low-loss metallic random systems. In fact, one of the earliest claims of AL of EM waves in 3D was made for a random system of aluminum spheres (28), but it was later retracted due to a large material absorption in the experiment (9). In SI, we argue that PEC model considered in our numerical simulation becomes justified for realistic metals at long wavelengths where field penetration depth is much shorter than particle size and wavelength. We suggest that (a) choice of a lower loss metal such as silver, (b) optimization of the sphere size and of the wavelength of EM waves, and (c) cooling to cryogenic temperatures to reduce loss (50) might be sufficient to realize 3D AL of light experimentally.

References

1. P. W. Anderson, Absence of diffusion in certain random lattices, *Phys. Rev.* **109**, 1492 (1958).
2. N. Mott, Electrons in disordered structures, *Adv. Phys.* **16**, 49 (1967).
3. B. Kramer, A. MacKinnon, Localization: theory and experiment, *Rep. Prog. Phys.* **56**, 1469 (1993).
4. M. Imada, A. Fujimori, Y. Tokura, Metal-insulator transitions, *Rev. Mod. Phys.* **70**, 1039 (1998).

5. J. Billy, *et al.*, Direct observation of Anderson localization of matter waves in a controlled disorder, *Nature* **453**, 891 (2008).
6. F. Jendrzejewski, *et al.*, Three-dimensional localization of ultracold atoms in an optical disordered potential, *Nat. Phys.* **8**, 398 (2012).
7. S. John, Electromagnetic absorption in a disordered medium near a photon mobility edge, *Phys. Rev. Lett.* **53**, 2169 (1984).
8. P. W. Anderson, The question of classical localization. A theory of white paint?, *Phil. Mag. B* **52**, 505 (1985).
9. A. A. Chabanov, M. Stoytchev, A. Z. Genack, Statistical signatures of photon localization, *Nature* **404**, 850 (2000).
10. T. Schwartz, G. Bartal, S. Fishman, M. Segev, Transport and Anderson localization in disordered two-dimensional photonic lattices, *Nature* **446**, 52 (2007).
11. M. Segev, Y. Silberberg, D. N. Christodoulides, Anderson localization of light, *Nat. Photonics* **7**, 197 (2013).
12. T. R. Kirkpatrick, Localization of acoustic waves, *Phys. Rev. B* **31**, 5746 (1985).
13. H. Hu, A. Strybulevych, J. H. Page, S. E. Skipetrov, B. A. van Tiggelen, Localization of ultrasound in a three-dimensional elastic network, *Nat. Phys.* **4**, 945 (2008).
14. E. Guazzelli, E. Guyon, B. Souillard, On the localization of shallow water waves by random bottom, *J. Phys. Lett.* **44**, 837 (1983).
15. P. Sheng, B. White, Z. Q. Zhang, G. Papanicolaou, *Scattering and Localization of classical waves in random media*, P. Sheng, ed., Directions in Condensed Matter Physics (World Scientific Publishing, 1990), pp. 563–619.

16. I. Z. Rothstein, Gravitational Anderson localization, *Phys. Rev. Lett.* **110**, 011601 (2013).
17. S. John, Localization of light, *Phys. Today* **44**, 32 (1991).
18. A. Lagendijk, B. van Tiggelen, D. S. Wiersma, Fifty years of Anderson localization, *Phys. Today* **62**, 24 (2009).
19. A. F. Ioffe, A. R. Regel, Non-crystalline, amorphous, and liquid electronic semiconductors, *Prog. Semicond.* **4**, 237 (1960).
20. J. Haberko, L. S. Froufe-Perez, F. Scheffold, Transition from light diffusion to localization in three-dimensional amorphous dielectric networks near the band edge, *Nat. Comm.* **11**, 4867 (2020).
21. T. van der Beek, P. Barthelemy, P. M. Johnson, D. S. Wiersma, A. Lagendijk, Light transport through disordered layers of dense gallium arsenide submicron particles, *Phys. Rev. B* **85**, 115401 (2012).
22. T. Sperling, *et al.*, Can 3D light localization be reached in ‘white paint’?, *New J. Phys.* **18**, 013039 (2016).
23. Y. Lahini, *et al.*, Anderson localization and nonlinearity in one-dimensional disordered photonic lattices, *Phys. Rev. Lett.* **100**, 013906 (2008).
24. S. E. Skipetrov, J. H. Page, Red light for Anderson localization, *New J. Physics* **18**, 021001 (2016).
25. S. E. Skipetrov, I. M. Sokolov, Absence of Anderson localization of light in a random ensemble of point scatterers, *Phys. Rev. Lett.* **112**, 023905 (2014).

26. B. A. van Tiggelen, S. E. Skipetrov, Longitudinal modes in diffusion and localization of light, *Phys. Rev. B* **103**, 174204 (2021).
27. L. A. Cobus, G. Maret, A. Aubry, Transient critical regime for light near the three-dimensional Anderson transition, *arXiv:2109.11188* (2021).
28. A. Z. Genack, N. Garcia, Observation of photon localization in a three-dimensional disordered system, *Phys. Rev. Lett.* **66**, 2064 (1991).
29. G. Watson Jr, P. Fleury, S. McCall, Searching for photon localization in the time domain, *Phys. Rev. Lett.* **58**, 945 (1987).
30. D. S. Wiersma, P. Bartolini, A. Lagendijk, R. Righini, Localization of light in a disordered medium, *Nature* **390**, 671 (1997).
31. M. Störzer, P. Gross, C. M. Aegerter, G. Maret, Observation of the critical regime near Anderson localization of light, *Phys. Rev. Lett.* **96**, 063904 (2006).
32. T. Sperling, W. Bührer, C. M. Aegerter, G. Maret, Direct determination of the transition to localization of light in three dimensions, *Nat. Photonics* **7**, 48 (2013).
33. S. Gentilini, A. Fratolocchi, L. Angelani, G. Ruocco, C. Conti, Ultrashort pulse propagation and the Anderson localization, *Opt. Lett.* **34**, 130 (2009).
34. L. Pattelli, A. Egel, U. Lemmer, D. S. Wiersma, Role of packing density and spatial correlations in strongly scattering 3D systems, *Optica* **5**, 1037 (2018).
35. Flexcompute inc. <https://flexcompute.com>, Accessed: 2021-12-31.
36. T. W. Hughes, M. Minkov, V. Liu, Z. Yu, S. Fan, A perspective on the pathway toward full wave simulation of large area metalenses, *Appl. Phys. Lett.* **119**, 150502 (2021).

37. L. Lu, J. D. Joannopoulos, M. Soljacic, Topological photonics, *Nat. Photonics* **8**, 821 (2014).
38. S. Stützer, *et al.*, Photonic topological Anderson insulators, *Nature* **560**, 461 (2018).
39. L. Sapienza, *et al.*, Cavity quantum electrodynamics with Anderson-localized modes, *Science* **327**, 1352 (2010).
40. D. S. Wiersma, Random quantum networks, *Science* **327**, 1333 (2010).
41. H. Cao, Y. Eliezer, Harnessing disorder for photonic device applications, *Appl. Phys. Rev.* (2022). To be published.
42. E. Akkermans, G. Montambaux, *Mesoscopic Physics of Electrons and Photons* (Cambridge University Press, Cambridge, UK, 2007).
43. S. E. Skipetrov, B. A. van Tiggelen, Dynamics of Anderson localization in open 3D media, *Phys. Rev. Lett.* **96**, 043902 (2006).
44. D. J. Thouless, Electrons in disordered systems and the theory of localization, *Phys. Rep.* **13**, 93 (1974).
45. J. B. Pendry, Quasi-extended electron states in strongly disordered systems, *J. Phys. C* **20**, 733 (1987).
46. E. Abrahams, P. W. Anderson, D. C. Licciardello, T. V. Ramakrishnan, Scaling theory of localization: Absence of quantum diffusion in two dimensions, *Phys. Rev. Lett.* **42**, 673 (1979).
47. C. A. Müller, D. Delande, *Ultracold Gases and Quantum Information: Lecture Notes of the Les Houches Summer School in Singapore* (Oxford University Press, 2011), chap. 9.

48. N. Cherroret, S. E. Skipetrov, B. A. van Tiggelen, Transverse confinement of waves in three-dimensional random media, *Phys. Rev. E* **82**, 056603 (2010).
49. H. C. van de Hulst, *Light scattering by small particles* (Dover, New York, 1981).
50. A. Z. Genack, A. A. Chabanov, Signatures of photon localization, *J. Phys. A* **38**, 10465 (2005).

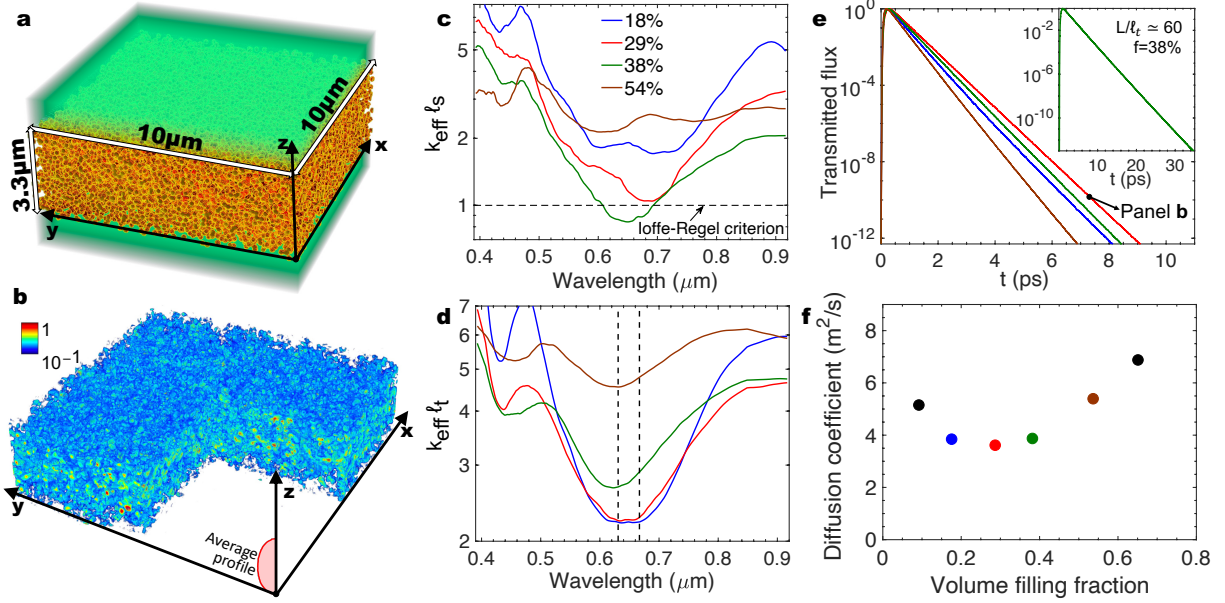


Figure 1: Absence of non-diffusive transport in random dielectric systems with index contrast of 3.5. a, 3D slab filled with dielectric spheres at random uncorrelated positions (radius $r = 100\ \text{nm}$, refractive index $n = 3.5$) in air. The slab cross-section is $10\ \mu\text{m} \times 10\ \mu\text{m} = 100\ \mu\text{m}^2$ and thickness is $L = 3.3\ \mu\text{m}$. b, 3D distribution of light intensity inside the slab (dielectric filling fraction $f = 29\%$, $L/\ell_t = 33$) at long delay time after a short pulse of plane wave front is incident on the front surface. Red curve with shading shows the average depth profile. c, Spectral dependence of the Ioffe-Regel parameter $k_{\text{eff}} \ell_s$ for different volume filling fractions of dielectric spheres, showing enhancement of scattering around single-sphere Mie resonances. The horizontal dashed line marks the Ioffe-Regel criterion $k_{\text{eff}} \ell_s = 1$ for 3D localization. d, Transport mean free path ℓ_t (in units of $1/k_{\text{eff}}$) as a function of wavelength, revealing a saturation by dependent scattering at high dielectric filling fractions. The vertical dashed lines mark spectral width (33 nm) of the excitation pulse in b and e. e, Transmittance of the 3D slab for a pulsed excitation, showing exponential decay in time for all dielectric filling fractions, in agreement with diffusive transport. Inset shows persistence of diffusion when L/ℓ_t is increased from 33 to 60 for $f = 38\%$, c.f. green line. f, Dependence of the minimum diffusion coefficient within the pulse bandwidth on the dielectric filling fraction f , exhibiting a minimum value of $3.6\ \text{m}^2/\text{s}$ at $f \simeq 29\%$.

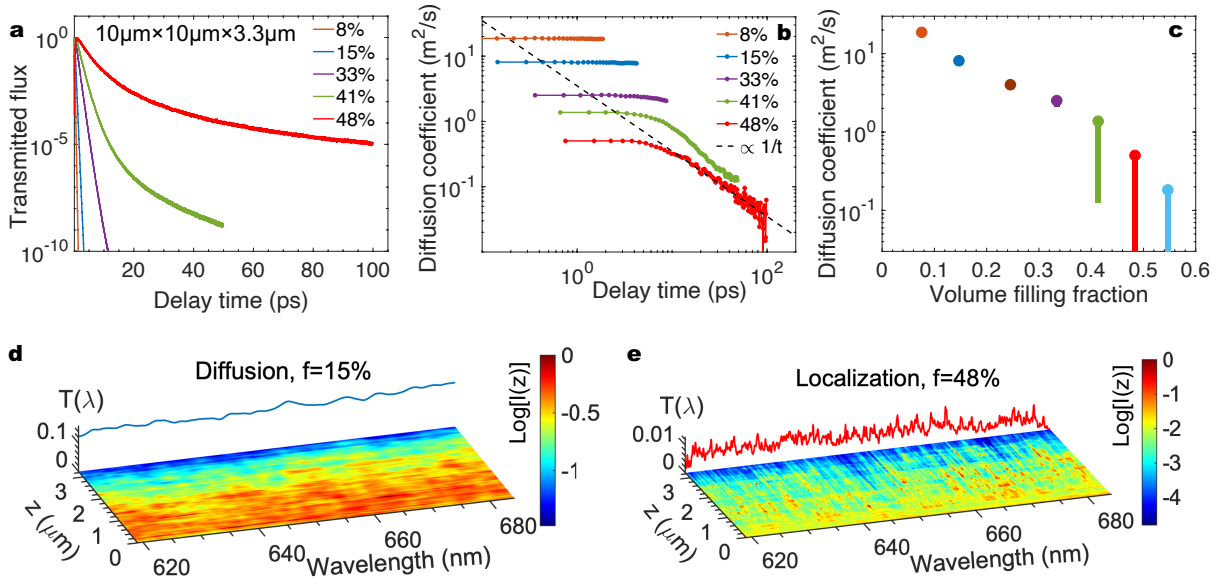


Figure 2: **3D Anderson localization of light in disordered PEC.** a, Transmittance $T(t)$ of an optical pulse through a 3D slab ($10\mu\text{m}\times 10\mu\text{m}\times 3.3\mu\text{m}$) of randomly packed PEC spheres with radius $r = 50$ nm and volume filling fractions f from 8% to 48%. b, Time-resolved diffusion coefficient $D(t)$ extracted from the decay rate of $T(t)$ in panel a, decreasing with time as $1/t$ at high f . c, Short-time D (dots) and the interval of variation of D with time (bars) at different f . d,e, Continuous-wave transmittance spectrum $T(\lambda)$ in diffusive (d, $f = 15\%$, blue line) and localized (e, $f = 48\%$, red line) PEC slabs. Color map: depth profile of average intensity $\langle I(x, y_0, z; \lambda) \rangle_x$ inside the slab at different wavelengths, highlighting the localized and necklace-like states for $f = 48\%$.

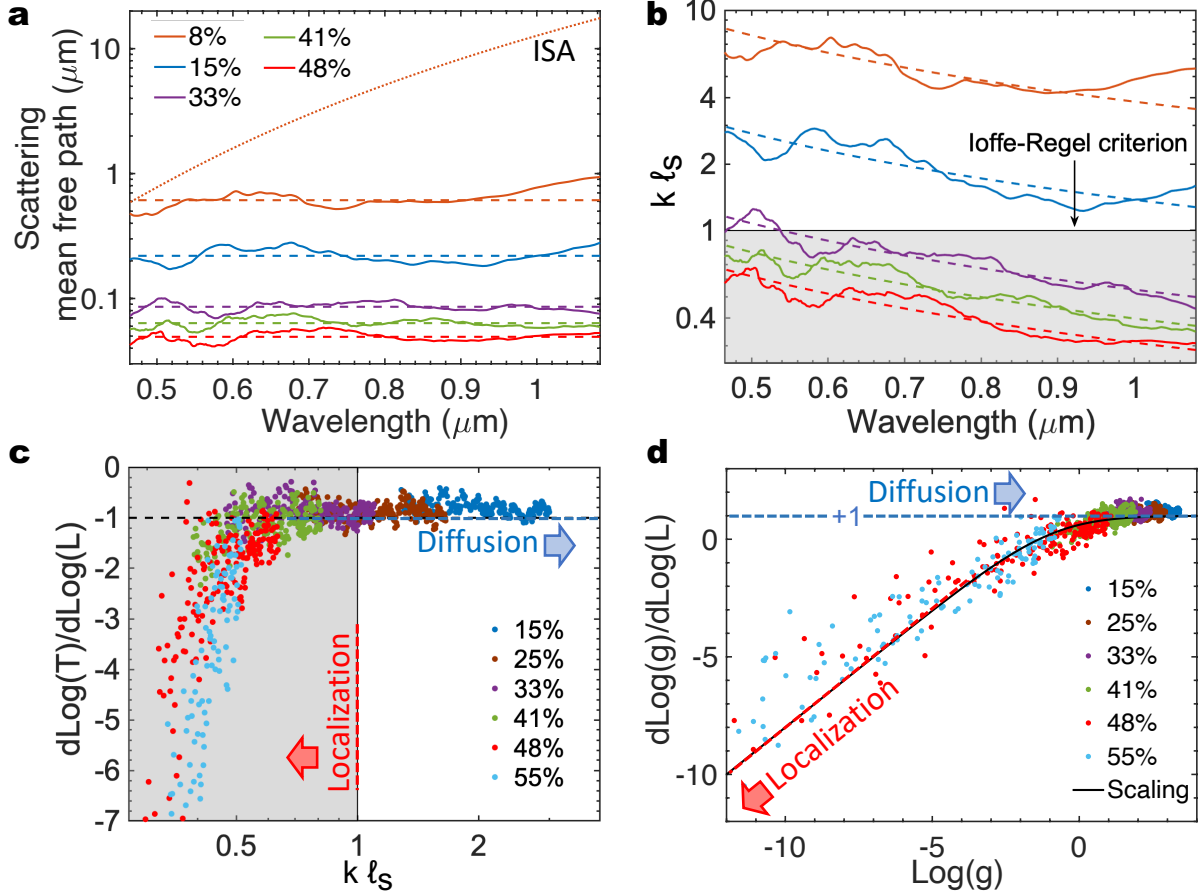


Figure 3: **Transition from diffusion to Anderson localization in disordered PEC.** a, Scattering mean free path ℓ_s for PEC volume filling fractions f from 8% to 48%. ℓ_s is nearly flat over broad spectral range. b, Spectral dependence of Ioffe-Regel parameter $k\ell_s$, exhibiting $1/\lambda$ dependence (dashed lines). c, Scaling of the continuous-wave (CW) transmittance T with slab thickness L versus Ioffe-Regel parameter $k\ell_s$, revealing diffusion-localization transition at $k\ell_s \sim 1$. Blue dashed line denotes diffusive scaling $T \propto L^{-1}$; red dashed line marks $k\ell_s = 1$. d, Single-parameter scaling of dimensionless conductance g for diffusion-localization transition (solid black line), in agreement with numerical data for 6 PEC filling fractions. Blue and red dashed lines denote diffusive and localized scalings $g \propto L$ and $g \propto \exp(-L/\xi)$ respectively, where ξ is the localization length.

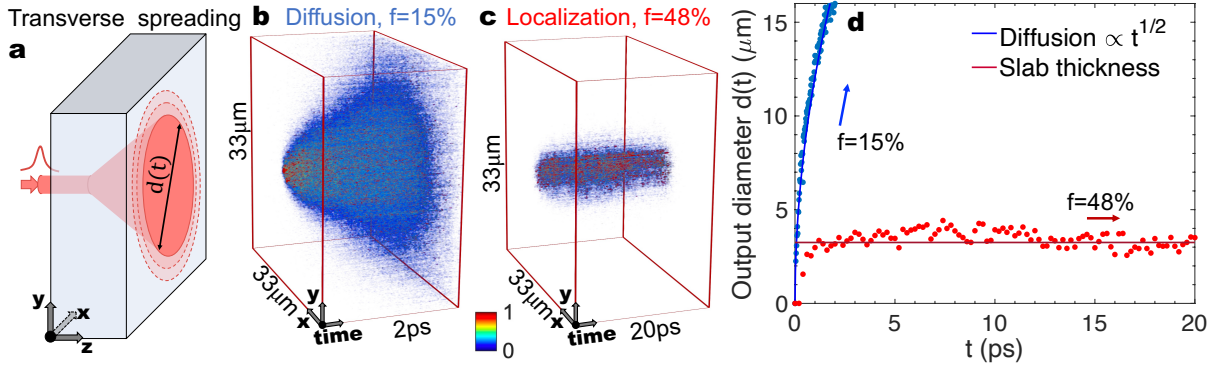


Figure 4: **Arrest of transverse spreading in 3D localized slab.** a, Schematic of transverse spreading of a narrow beam propagating through a diffusive slab of cross section $33 \mu\text{m} \times 33 \mu\text{m}$ and thickness $L = 3.3 \mu\text{m}$. b, 2D intensity distribution at the output surface (normalized to the maximum) for different delay times, showing a lateral expansion of the beam in the diffusive slab of PEC filling fraction $f = 15\%$. c, Absence of transverse spreading for $f = 48\%$, due to Anderson localization. d, Lateral diameter of the transmitted beam $d(t)$ increases as \sqrt{t} in the diffusive slab (blue dots), but it saturates to the slab thickness L in the localized slab (red dots).

Acknowledgments

This work is supported by the National Science Foundation under Grant Nos. DMR-1905465, DMR-1905442, and the Office of Naval Research (ONR) under Grant No. N00014-20-1-2197.

Author contributions

A.Y. performed numerical simulations, analyzed the data and compiled all results. S.E.S. conducted theoretical study and guided data interpretation. T.W.H. and M.M. implemented the hardware-accelerated FDTD method and aided in the setup of the numerical simulations. Z.Y. and H.C. initiated this project and supervised the research. A.Y. wrote the first draft, S.E.S. and H.C. revised the content and scope, T.W.H. and M.M. and Z. Y. edited the manuscript. All co-authors discussed and approved the content.